Supplementary Information: *In* situ three-dimensional observation of plasticity onset in a Pt nanoparticle

Sarah Yehya*[1,2,3], Thomas W. Cornelius[1], Marie-Ingrid Richard[2,4], Felisa Berenguer[3], Mor Levi[5], Eugen Rabkin[5], Olivier Thomas[1], and Stéphane Labat[1]

[1]Aix-Marseille Université, Université de Toulon, CNRS, IM2NP, Marseille, France
[2]Univ. Grenoble Alpes, CEA Grenoble, IRIG, MEM, NRX, 17 avenue des Martyrs, F-38000 Grenoble, France
[3]Synchrotron SOLEIL - L'Orme des Merisiers, Saint-Aubin, BP 48 FR - 91192 Gif-sur-Yvette, France
[4]ID01/ESRF - The European Synchrotron, 71 Avenue des Martyrs, 38000 Grenoble, France
[5]Department of Materials Science and Engineering, Technion - Israel Institute of Technology, 3200003 Haifa, Israel

BCDI

During Bragg Coherent X-ray Diffraction Imaging, the 3D intensity distribution can be mapped in the reciprocal space by recording the scattered intensity from crystals on a 2D detector in the far-field regime. Only the intensity of the diffracted wavefield is measured while its phase is missing. In order to Fourier transform back the diffraction data of one Bragg peak and access the morphology and strain fields of a crystal in the real space, the knowledge of both amplitude and phase is mandatory. The studied crystal must be well isolated and smaller than the coherence volume of the monochromatic beam. Additionally, the diffraction pattern has to be oversampled at least twice the Nyquist frequency, *i.e.* satisfying Shannon's principle [1]. Under these conditions, the complex part of the electron density can be recovered relying on phase retrieval algorithms. The reconstructed electron density was obtained using the PyNX package [2]. The iterative phase retrieval algorithm starts with an initial guess of the phase then Fourier transform iterations are performed between direct and reciprocal spaces by applying constraints (such as finite support, shrink wrap, *etc*) until converging to a solution. Once the missing phase of the complex electron density is recovered, it gives access to the displacement field (proportional to the retrieved phase) as well as the strain field which is the gradient of the displacement field projected onto the scattering vector. The diffraction data was pre- and post-processed using the BCDI package[3].

Simulation

COMSOL Multiphysics software was used for Finite Element Method simulation. The shape of the Pt nanoparticle before indentation was retrieved from the 3D reconstruction of the BCDI measurement. The former is then used in the simulation while adding a sapphire substrate to the Pt NP to obtain accurate results. Anisotropic elastic constants of Pt were used in the simulation with C_{11} = 347 GPa, C_{12} = 251 GPa and C_{44} = 76 GPa in Voigt notation reference. Then a surface having a radius of 20 nm was defined on the top facet of the Pt particle where then a force of 5.5 µN was applied to mimic the AFM tip/indent. All the surfaces are defined as free surfaces except the bottom surface of the Sapphire substrate that has been fixed. But actually, the simulation did not include the initial residual strain of the particle. Therefore, this initial deformation (see the 1st image of Fig. 2) was removed from experimental phase field shown in Fig. 3j. It is noteworthy that the color bar values in Fig.(5a) are smaller than those in Fig.(5b) owing to the fact that the reconstruction has been obtained while the AFM tip was still held on top of the particle, for which the algorithm has not been able to converge to a solution at the contact between the tip and the surface (see white in Fig. 5a). Nevertheless, in BCDI we only measure the local, inhomogeneous relative strain while in simulation the global strain is calculated on that account, an average strain must be removed from the simulation in furtherance of comparing it to the experimental one. This latter comes back to removing a slope on the experimental phase field.

Supplementary figures

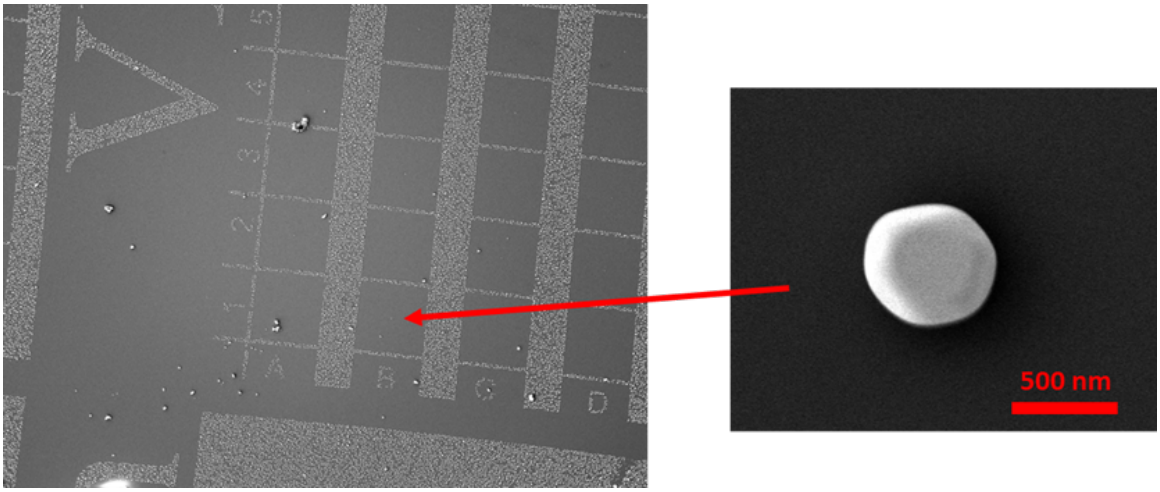

Figure S1: SEM images showing the patterned sample and one isolated Pt particle at each square of 100 x 100 μm^2.

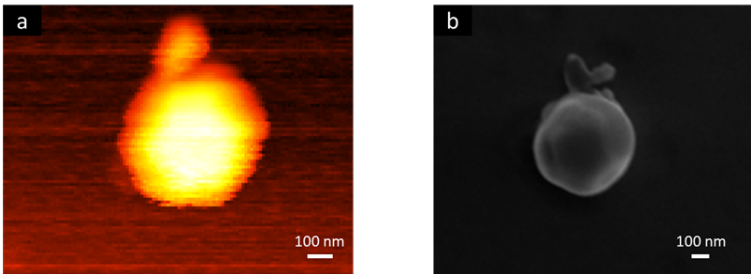

Figure S2: (a) AFM topography image of the selected Pt nanoparticle taken before indentation, (b) SEM image taken of the particle after indentation. We notice also an impurity located near the particle in the SEM and AFM images.

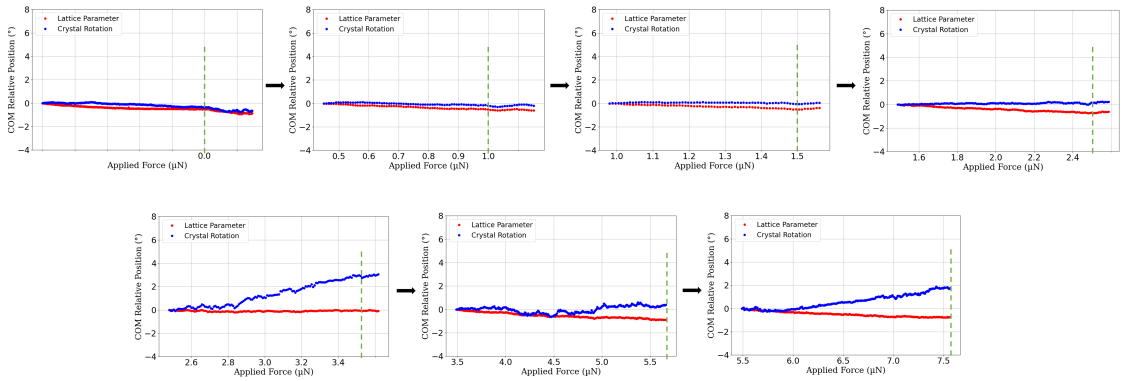

Figure S3: Center of mass (C.O.M.) relative position of the monitored **111** 2D Bragg peak of the Pt NP during the first indentation. (blue dots represent the crystal rotation and the red dots represent the lattice parameter)

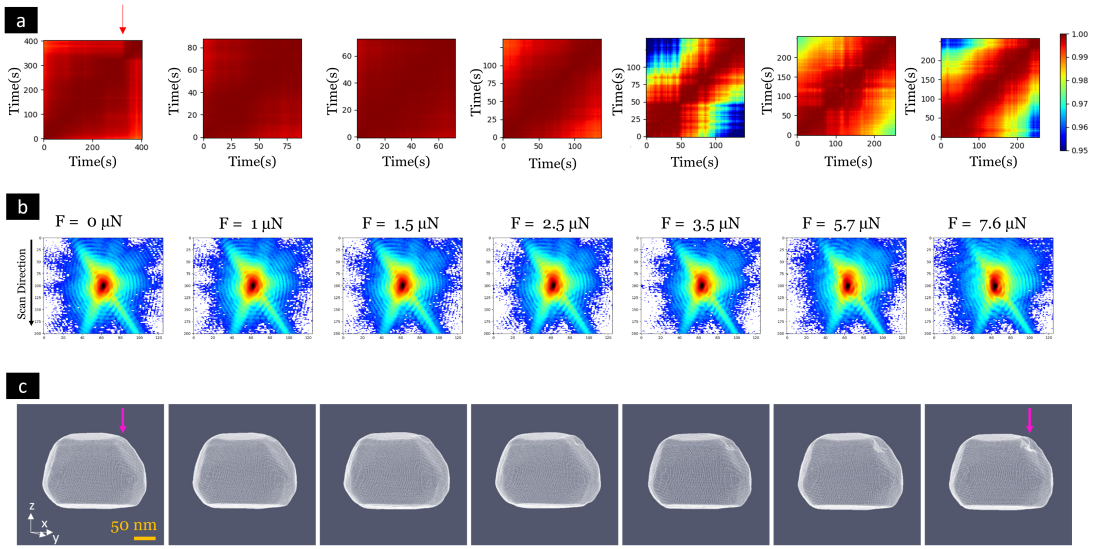

Figure S4: (a) Cross-correlation of the 2D BCDP taken during the first indentation. (b) 3D diffraction patterns recorded at each loading step while maintaining the applied force. (d) 3D semi-transparent rendering of the particle during indentation at each loading step, evidencing no defect inside.

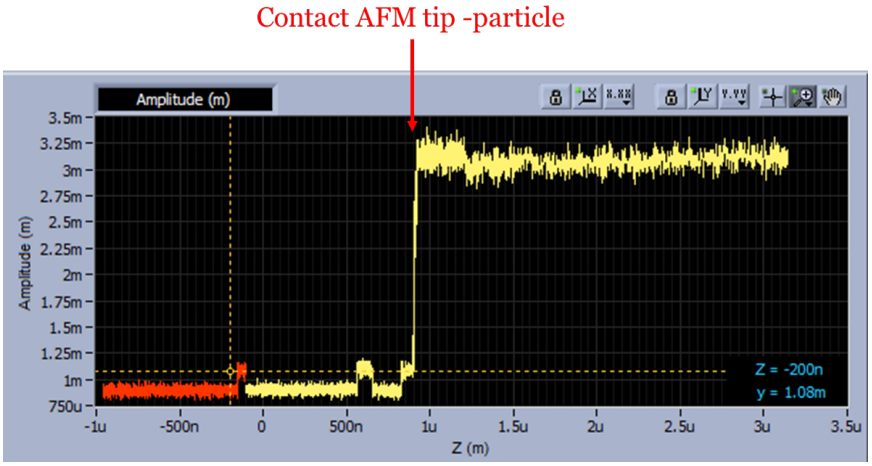

Figure S5: Approach curve of the AFM piezoelectric head vs. the Amplitude of the oscillating cantilever. Once the AFM tip hits the Pt surface (see red arrow), oscillations of the cantilever are damped and the amplitude drops sharply indicating that the tip is in contact with the particle.

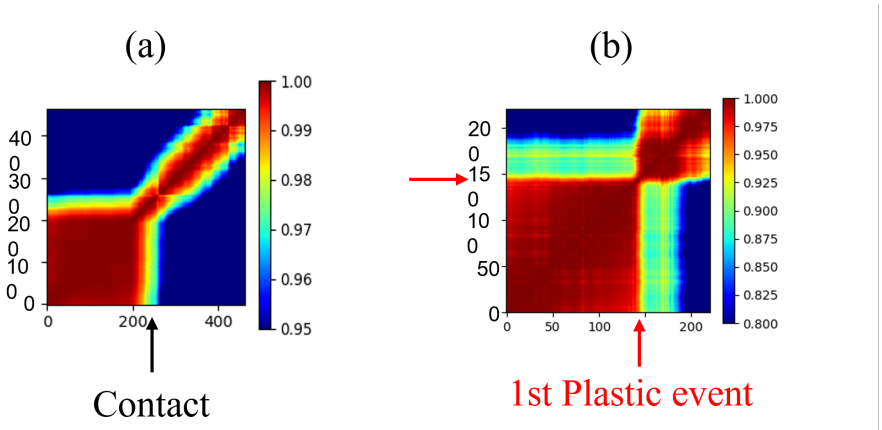

Figure S6: Cross-correlation matrix of 2D Bragg Coherent Diffraction patterns (a) reaching and applied force of 5.5 μN and (b) reaching an applied force of 9.9μN.

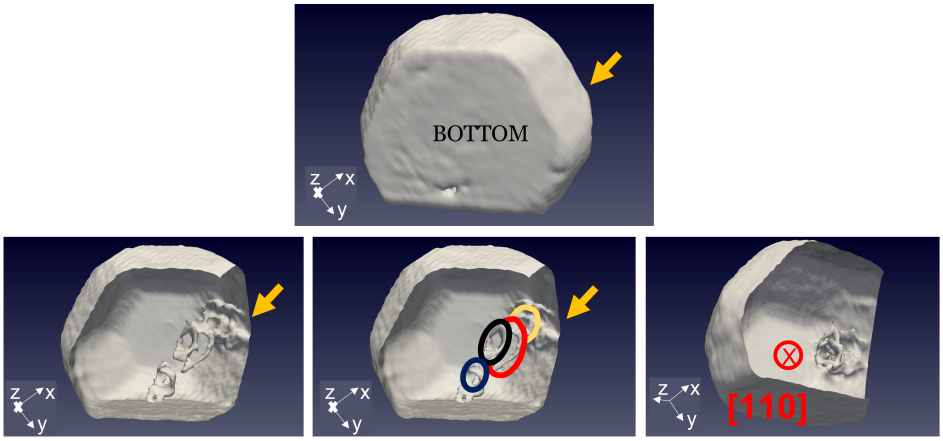

Figure S7: Arrangement of the inner defects during an applied force of 9.9 µN, showing also the imprint of the AFM-tip (by yellow arrow).

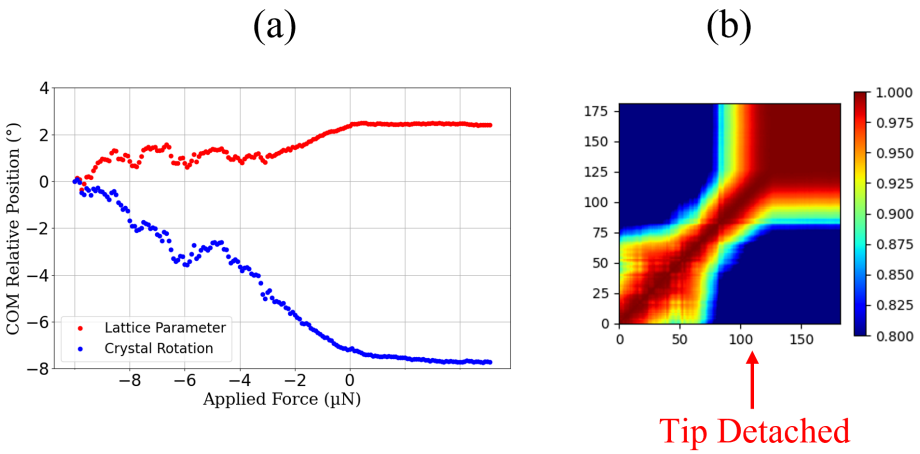

Figure S8: (a) Average Bragg peak position and (b) cross-correlation matrix of the 3D Bragg Coherent Diffraction pattern upon unloading.

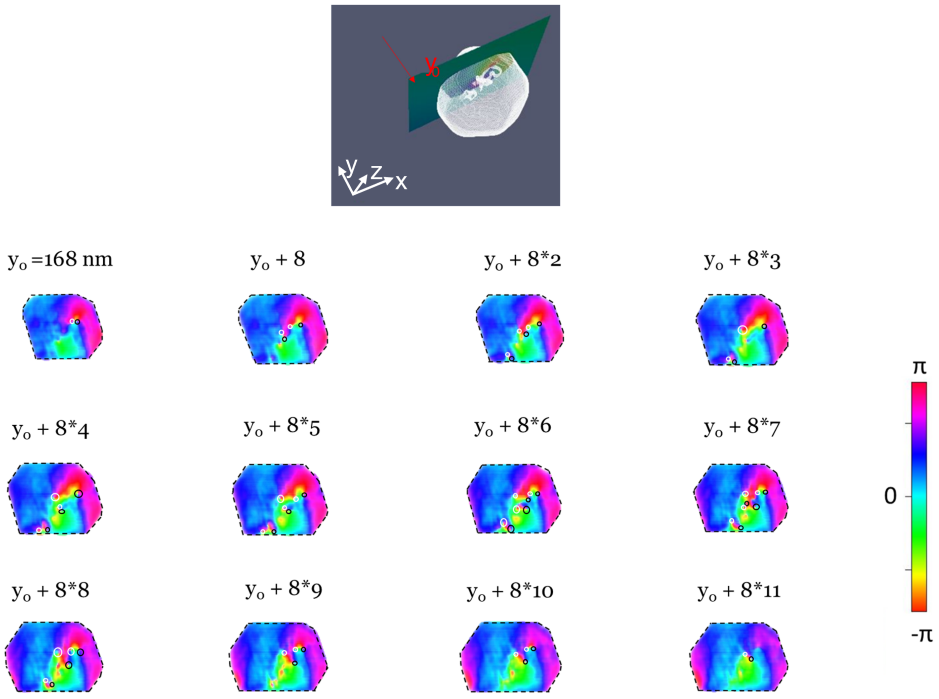

Figure S9: 2D slices of the reconstructed phase field along the [111] of the Pt particle displaying the 2π phase vortices of induced dislocations.

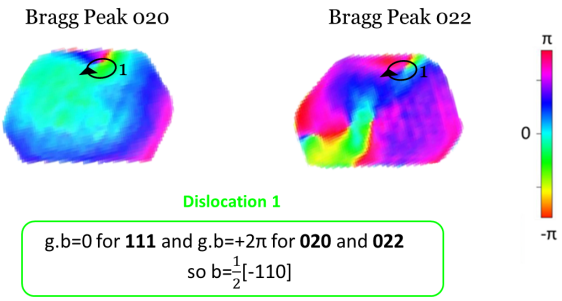

Figure S10: The ambiguity on the sign of the inferred Burgers vector from g.b contrast is overcome by following the sign of the 2π phase vortices surrounding corresponding dislocations.

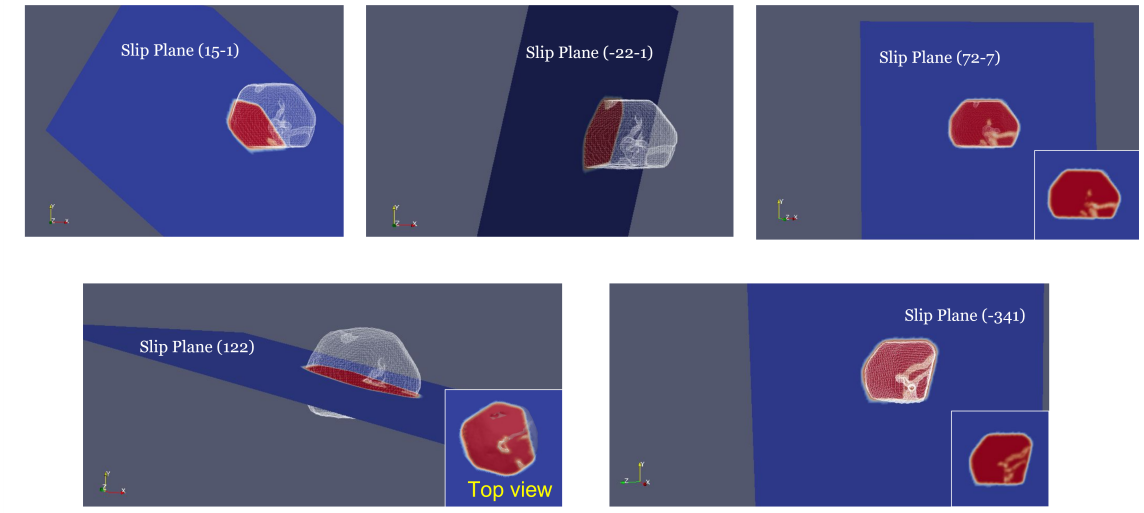

Figure S11: Slip planes containing dislocation arms and loops of the induced defects after combining all reflections.

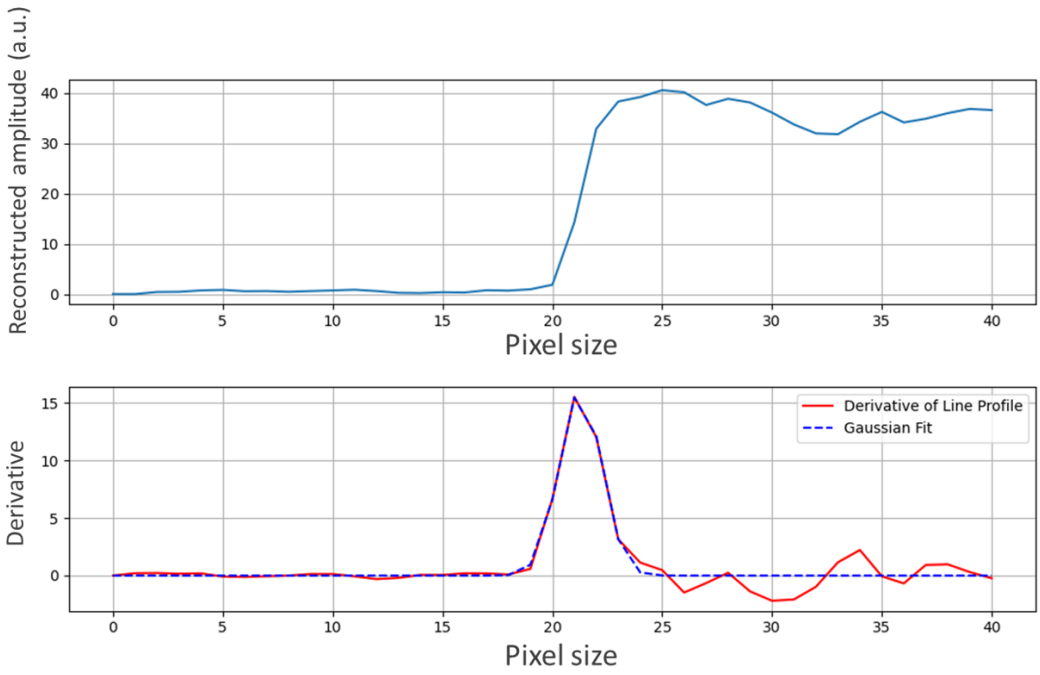

Figure S12: (a) Line profile of the amplitude of the reconstructed electron density across the crystal-substrate interface.(b) Derivative of the line profile. The spatial resolution of the reconstructed diffraction data was recovered by fitting the derivative with a Gaussian, where 2σ is taken as the average 3D spatial resolution and corresponds to 18 nm. The pixel size is equal to 9 nm.

References

[1] David Sayre. Some implications of a theorem due to shannon. Acta Crystallographica, 5(6):843–843, 1952.

[2] Vincent Favre-Nicolin, Johann Coraux, M-I Richard, and Hubert Renevier. Fast computation of scattering maps of nanostructures using graphical processing units. Journal of Applied Crystallography, 44(3):635–640, 2011.

[3] Bcdi python package,. `https://doi.org/10.5281/zenodo.3257616`.